



# Impact of micro-alloying on the plasticity of Pd-based bulk metallic glasses



Niklas Nollmann, Isabelle Binkowski, Vitalij Schmidt, Harald Rösner\*, Gerhard Wilde

Institut für Materialphysik, Westfälische Wilhelms-Universität Münster, Wilhelm-Klemm-Str. 10, D-48149 Münster, Germany

## ARTICLE INFO

### Article history:

Received 13 August 2015

Accepted 26 August 2015

Available online 1 September 2015

### Keywords:

Bulk metallic glass  
Mechanical properties  
Plastic deformation  
Ductility  
Shear bands

## ABSTRACT

Micro-alloying was performed using additions of Co and Fe to monolithic Pd<sub>40</sub>Ni<sub>40</sub>P<sub>20</sub> bulk metallic glass. Compression tests showed a plastic strain of 13% for the Co addition (1 at.%), whereas the Fe addition (0.6 at.%) led to immediate failure after reaching the elastic limit. Plasticity is not reflected by the high Poisson's ratio of 0.4 since it remained unaffected by minor alloying. Applying the fictive temperature concept to analyze the impact of minor alloying suggests that the total amount of free volume frozen-in during vitrification is less important for the mechanical properties of bulk metallic glasses than its local distribution.

© 2015 Acta Materialia Inc. Published by Elsevier Ltd. All rights reserved.

Bulk metallic glasses (BMGs) show unique mechanical properties such as high strength, extended elasticity, high wear and corrosion resistance [1]. However, the limited ductility and especially the immediate catastrophic failure in tension after reaching the elastic limit are major obstacles for BMGs as structural materials [1]. The limited ductility has led to substantial effort in order to improve the plasticity of BMGs. The design of composites [2–7] composed of ductile crystalline phase in a BMG matrix has been proposed as a promising way to overcome the limited ductility. Moreover, monolithic glasses with high Poisson's ratios near the ideal value of 0.5 are reported to have improved compressive and bending plasticity [8–12]. Thus, the value of the Poisson's ratio had been suggested as an indicator for ductile or brittle behavior [9]. In addition, it was observed that materials with a high Poisson's ratio form a high number of fine-dispersed shear bands [10,12]. However, small changes in the alloy composition called minor- or micro-alloying were found to cause major changes with respect to the glass forming ability, thermal stability and plasticity of BMGs [13,14]. Drastic changes of the ductility upon thermal relaxation in the glass transition region without accompanying changes of the elastic constants have also been reported [15,16] and a model based on the relation between the glass transition temperature and a critical fictive temperature has been suggested to rationalize the effects of thermal relaxation and composition on room temperature plasticity of metallic glasses [17]. The fictive temperature concept represents, according to Tool and Eichlin

[18], a measure of the relaxation state of a glassy material and thus, in the framework of free-volume based models, a measure of the relative amount of free volume stored in the material. In this study, micro-alloying was applied to the well-known glass-former Pd<sub>40</sub>Ni<sub>40</sub>P<sub>20</sub> which shows high kinetic stability against crystallization and phase separation [19,20]. Starting from the 'classical' ternary system, micro-alloying was carried out using Co and Fe as additives. Their mechanical responses showed completely opposite effects regarding the ductility. The corresponding Poisson's ratios were determined but found to be unaffected by the compositional changes. This raises several questions that need to be addressed: (i) Is the Poisson's ratio the only property that characterizes the ductility? (ii) What hinders the shear bands from propagating through the material and causing catastrophic failure? (iii) What changes are introduced in the glass by minor alloying?

Ingots of Pd<sub>40</sub>Ni<sub>40</sub>P<sub>20</sub> were produced by ingot copper mold casting in a melt spinner under argon atmosphere. The initial alloy compound was modified by adding 1 at.% Co or 0.6 at.% Fe to the ternary system. Before casting, the ingots were cycled with boron oxide (B<sub>2</sub>O<sub>3</sub>) to purify the sample. The sizes of the as-cast ingots were 3 mm (diameter) × 30 mm (length) for uniaxial compression tests and 30 mm (length) × 10 mm (width) × 1 mm (height) for the three-point bending tests. After casting, the ingots were cut with a diamond wire saw to sample dimensions of 4 mm (length) × 3 mm (diameter) providing a 4:3 aspect ratio for the uniaxial compression tests in accordance with the accepted specification for mechanical tests [21]. The three-point bending experiments were carried out with samples cut to dimensions of 10 mm (length) × 1 mm (width) × 1 mm (height). Uniaxial

\* Corresponding author.

E-mail address: [rosner@uni-muenster.de](mailto:rosner@uni-muenster.de) (H. Rösner).

compression and bending tests were performed in a screw-driven mechanical test instrument (Instron model 1195) equipped with extra hardened anvils made from Böhler S290 microclean steel. The uniaxial compression tests were performed using a strain rate of  $2.5 \times 10^{-5} \text{ s}^{-1}$  and the three-point bending tests were carried out at a strain rate of  $10^{-3} \text{ s}^{-1}$ . The reliability of the deformation data was ensured by testing five samples for each composition.

X-ray studies were performed with a Siemens D5000 X-ray diffractometer using Cu K $\alpha$  radiation to confirm the overall amorphous state of the samples (cf. Fig. 1(a)). In addition, energy-filtered diffraction patterns were acquired with an Omega in-column filter using a slit width of 10 eV to confirm the presence of the glassy state without local nano-crystallization. The illuminated area contributing to the diffraction information was  $0.5 \mu\text{m}^2$  using an exposure time of 1 s. The PASAD tool [22] was used to extract the annular profiles shown in Fig. 1(b).

Calorimetric measurements were performed on as-quenched samples with a differential scanning calorimeter (Perkin Elmer Diamond DSC) using a heating rate of 20 K/min to monitor the glass transition and crystallization temperature. The fictive temperature concept was applied following the idea of Tool and Eichlin [18]. In order to estimate the fictive temperature,  $T_{\text{fict}}$ , as-quenched samples were heated at 20 K/min to 630 K, which is well above the glass transition, and subsequently cooled at a controlled cooling rate down to 300 K. After holding the sample at 300 K for 10 min, the DSC loop was repeated for different cooling rates (10, 20, 40 and 60 K/min). This procedure yields different values for  $T_{\text{fict}}$  depending on the prior cooling cycle and thus displays the relaxation of the (frozen-in) state of the previous cooling cycle giving a measure for the amount of free volume stored in the glass.

The microstructure of the BMG was characterized by optical microscopy (Keyence VHX-500K), scanning electron microscopy (Nova Nano230SEM) and transmission electron microscopy (Zeiss Libra 200FE) using electro-polishing with a BK-2 electrolyte [23] for the preparation of electron-transparent samples.

The Poisson's ratios were determined from ultrasonic measurements carried out with an Olympus 38DL Plus device.

The glassy structure of different as-cast  $\text{Pd}_{40}\text{Ni}_{40}\text{P}_{20}$  alloys with and without additions of Co or Fe was confirmed by X-ray diffraction (XRD) (Fig. 1(a)) and locally by selected area electron diffraction (SAED) taken from different sample areas (Fig. 1(b)). They all display the typical X-ray amorphous characteristics of BMGs. No crystalline phases or indications for phase separation were found. As expected for minor additions of Fe or Co, there were no observed shifts in the diffraction maxima of the XRD and SAED pattern.

The calorimetric results are displayed in Fig. 2 and summarized in Table 1. The glass transition temperature  $T_g$  (defined as the onset

temperature) seems not to be strongly affected by micro-alloying. The crystallization temperature  $T_x$  was raised by the minor alloying leading to an increase of  $\Delta T = T_x - T_g$ . However, since the onset of crystallization is affected strongly by different factors such as the purity and purification of the material, the cooling rate and melt superheating temperature or, as recently shown [24] by annealing the glass near room temperature, the absolute value of  $\Delta T$  bears no significant meaning.

The results of the mechanical testing are shown in Fig. 3. The original ternary  $\text{Pd}_{40}\text{Ni}_{40}\text{P}_{20}$  alloy already shows a plastic strain of more than 9% in compression (cf. Fig. 3(a)). This appears to contradict a former report where only 0.4% of plastic strain was reported for this compound [25]. However, the reported tests were carried out with rectangular shaped samples having an aspect ratio of 3:1 and were thus different in that case. Co addition (1 at.%) leads to an increase in plastic strain of about 50%, whereas the material with Fe addition (0.6 at.%) immediately shows catastrophic failure after reaching the elastic limit. It was shown that the activation of shear bands can be directly linked to the flow serrations in uniaxial compression tests [26]. We thus assume that the formation of each such major shear band is manifested in a single serration during the uniaxial compression test (cf. Fig. 3(a)).

Since compression tests have been shown to be indecisive in determining plasticity in metallic glasses mainly due to the sensitivity of alignment and sample geometry [27], three-point bending tests were performed in addition. A video recording the progress of bending for the Co containing alloy in time-lapse can be found in the Appendix A. To access this video component, simply click on the link (online version only).

An increased ductility was found (cf. Fig. 3(b)) making it impossible to deform the Co containing samples to failure (Video 1). Thus it is worth noting that the end of the curve for the Co containing alloy in Fig. 3(b) does not display the failing of the sample rather than the maximum limit of bending in the testing device. However, it also should be mentioned that if according to Conner et al. [28] thicker samples had been used, it could have been possible to deform the Co containing samples to failure. Fig. 3(c) shows a SEM micrograph of a  $\text{Pd}_{40}\text{Ni}_{40}\text{P}_{20}$  bending sample after failure. There are long primary shear bands visible for the upper part (tensile state) of the bent sample and additionally secondary and tertiary shears bands branching off. However there is one major shear band that, apart from the one causing the failure, reaches the neutral fiber. The lower part, which displays the compressive state, shows many fine-dispersed shear bands and only very few long shear bands (dark contrast) as found in the upper part. Fig. 3(d) shows a SEM micrograph of a bent but not broken  $(\text{Pd}_{40}\text{Ni}_{40}\text{P}_{20})_{99}\text{Co}_1$  sample revealing the differences. There are also long primary shear bands visible for the upper part (tensile state)

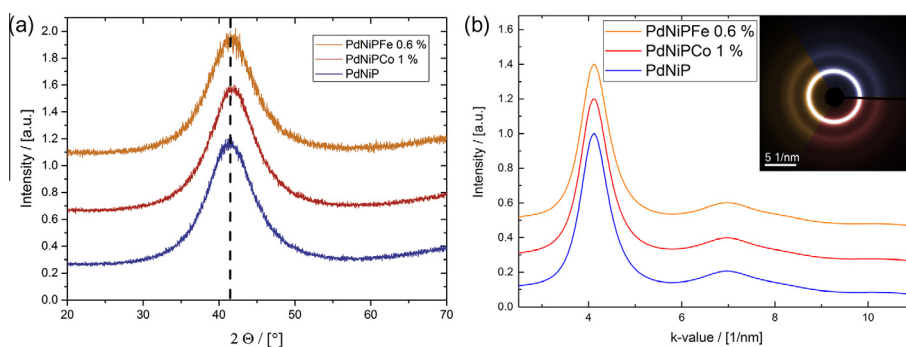


**Fig. 1.** (a) XRD pattern of  $\text{Pd}_{40}\text{Ni}_{40}\text{P}_{20}$  (red),  $(\text{Pd}_{40}\text{Ni}_{40}\text{P}_{20})_{99}\text{Co}_1$  (orange) and  $(\text{Pd}_{40}\text{Ni}_{40}\text{P}_{20})_{99.4}\text{Fe}_{0.6}$  (blue). (b) Energy-filtered SAED pattern of  $\text{Pd}_{40}\text{Ni}_{40}\text{P}_{20}$  (blue),  $(\text{Pd}_{40}\text{Ni}_{40}\text{P}_{20})_{99}\text{Co}_1$  (red) and  $(\text{Pd}_{40}\text{Ni}_{40}\text{P}_{20})_{99.4}\text{Fe}_{0.6}$  (orange) shown as annular profiles of the rings (inset). (For interpretation of the references to color in this figure legend, the reader is referred to the web version of this article.)

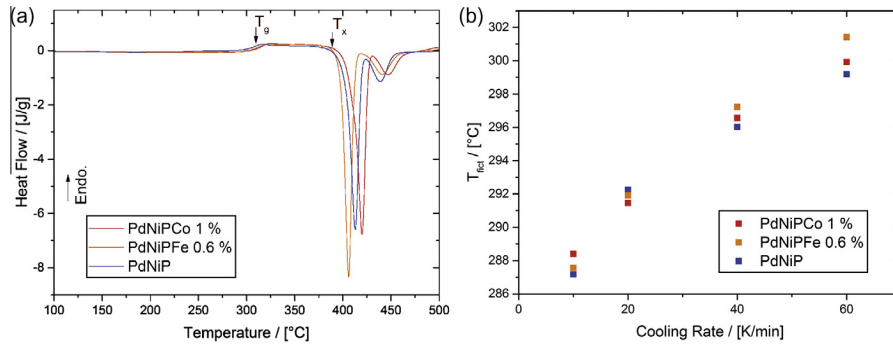


**Fig. 2.** (a) DSC charts of  $\text{Pd}_{40}\text{Ni}_{40}\text{P}_{20}$ ,  $(\text{Pd}_{40}\text{Ni}_{40}\text{P}_{20})_{99}\text{Co}_1$  and  $(\text{Pd}_{40}\text{Ni}_{40}\text{P}_{20})_{99.4}\text{Fe}_{0.6}$  using a heating rate of 20 K/min. (b) The cooling rate dependence of  $T_{fict}$  of  $\text{Pd}_{40}\text{Ni}_{40}\text{P}_{20}$ ,  $(\text{Pd}_{40}\text{Ni}_{40}\text{P}_{20})_{99}\text{Co}_1$ , and  $(\text{Pd}_{40}\text{Ni}_{40}\text{P}_{20})_{99.4}\text{Fe}_{0.6}$ .

**Table 1**

The enthalpy of crystallization  $\Delta H_x$ , glass transition temperature  $T_g$ , crystallization temperature  $T_x$ ,  $\Delta T$  defined as  $T_x - T_g$ , and the fictive temperature  $T_{fict}$  of the as-quenched samples of the DSC measurements shown in Fig. 2.

Sample	$T_g$ (°C)	$T_x$ (°C)	$\Delta T$ (°C)	$\Delta H_x$ (J/g)	$T_{fict}$ (°C)
$(\text{Pd}_{40}\text{Ni}_{40}\text{P}_{20})_{99}\text{Co}_1$	312.6	382.9	70.3	101.9	342.7
$(\text{Pd}_{40}\text{Ni}_{40}\text{P}_{20})_{99.4}\text{Fe}_{0.6}$	313.0	386.8	73.8	97.7	352.9
$\text{Pd}_{40}\text{Ni}_{40}\text{P}_{20}$	308.8	372.6	63.8	107.3	351.3

of the bent sample and additionally secondary and tertiary shear bands branching off. However, none of the long major shear bands crosses the neutral fiber. Thus, there must be a mechanism operating which hinders the major shear bands from propagating through the whole sample. We think that the highly branched state with many secondary and tertiary shear bands involved represents the mechanical response of the material to local modifications of the energy landscape. This highly branched state prevents the primary shear bands from spreading further and thus the material from failure. The lower part, which displays the compressive state,

shows again many fine-dispersed shear bands but fewer major shear bands. In contrast, the sample with the Fe addition (not shown) shows no shear bands since it fails with the initiation of the first shear band running through the whole sample.

While analyzing the dependence of the ductility of the present glasses on relaxation treatments, we utilize the fictive temperature concept to investigate the impact of minor alloying on the relative amount of free volume,  $\rho_v$ . This allows to compare the trend between  $\rho_v$  and the observed ductility for the present samples with the model suggested by Kumar et al. [17]. In fact, it is an open question, if the ductility of a metallic glass is governed by the absolute/relative amount of free volume present or by local atomic configurations or motifs [29], which may be modified by minor alloying.

Calorimetric analyses of DSC data served to estimate  $T_{fict}$  for each composition as a function of the cooling rate (cf. Fig. 2(b)). We found that after initial quenching  $T_{fict}$  and hence the relative amount of free volume was largest for the  $(\text{Pd}_{40}\text{Ni}_{40}\text{P}_{20})_{99.4}\text{Fe}_{0.6}$  alloy and smallest for the  $(\text{Pd}_{40}\text{Ni}_{40}\text{P}_{20})_{99}\text{Co}_1$  alloy (Table 1). The dependence of  $T_{fict}$  on the cooling rate of the previous vitrification run (cf. Fig. 2

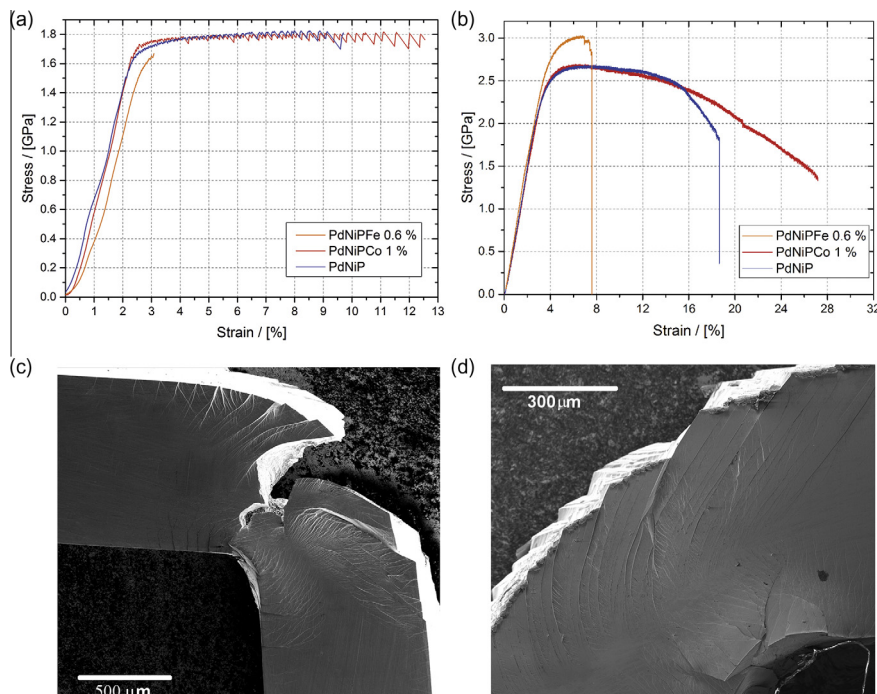


**Fig. 3.** (a) Compressive stress–strain curves of  $\text{Pd}_{40}\text{Ni}_{40}\text{P}_{20}$ ,  $(\text{Pd}_{40}\text{Ni}_{40}\text{P}_{20})_{99}\text{Co}_1$  and  $(\text{Pd}_{40}\text{Ni}_{40}\text{P}_{20})_{99.4}\text{Fe}_{0.6}$ . (b) Three-point bending tests: stress–strain curves of  $\text{Pd}_{40}\text{Ni}_{40}\text{P}_{20}$ ,  $(\text{Pd}_{40}\text{Ni}_{40}\text{P}_{20})_{99}\text{Co}_1$  and  $(\text{Pd}_{40}\text{Ni}_{40}\text{P}_{20})_{99.4}\text{Fe}_{0.6}$ . (c) SEM micrograph of a  $\text{Pd}_{40}\text{Ni}_{40}\text{P}_{20}$  sample after failure showing shear band details at the bending position. (d) SEM micrograph of bent  $(\text{Pd}_{40}\text{Ni}_{40}\text{P}_{20})_{99}\text{Co}_1$  sample showing shear band details at the bending position.

**Table 2**

Poisson's ratios of  $\text{Pd}_{40}\text{Ni}_{40}\text{P}_{20}$ ,  $(\text{Pd}_{40}\text{Ni}_{40}\text{P}_{20})_{99}\text{Co}_1$  and  $(\text{Pd}_{40}\text{Ni}_{40}\text{P}_{20})_{99.4}\text{Fe}_{0.6}$  determined from ultrasonic measurements.

Sample	Poisson ratio
$(\text{Pd}_{40}\text{Ni}_{40}\text{P}_{20})_{99}\text{Co}_1$	$0.403 \pm 0.001$
$(\text{Pd}_{40}\text{Ni}_{40}\text{P}_{20})_{99.4}\text{Fe}_{0.6}$	$0.402 \pm 0.001$
$\text{Pd}_{40}\text{Ni}_{40}\text{P}_{20}$	$0.400 \pm 0.001$

(b)) is similar for the three different alloys. Particularly, the absolute values of the fictive temperatures for the as-quenched states of the ternary- and the Fe-containing alloys are akin (Table 1), although their mechanical behavior differs strongly (cf. Fig. 3). Additionally, for all compositions the fictive temperature in the as-cast state is well above the glass temperature. These results indicate that the total amount of free volume frozen-in during vitrification is less important for the mechanical properties of bulk metallic glasses than the local distribution of free volume and thus the spectrum of local atomic configurations or motifs [29].

The Poisson's ratios measured are shown in Table 2. For the ternary  $\text{Pd}_{40}\text{Ni}_{40}\text{P}_{20}$  glass, we obtain a value of 0.400 which correlates well with other measurements [30,31]. However, the Poisson's ratios of the samples containing Co or Fe do not show changes within the measuring error. Thus brittle or ductile behavior can exist at almost identical Poisson's ratios. This result confirms former reports [12,15,16] that are in disagreement with the finding of Lewandowski et al. [9] that Poisson's ratio is an indicator for plastic and brittle behavior of a bulk metallic glass.

Two new  $\text{Pd}_{40}\text{Ni}_{40}\text{P}_{20}$  based metallic glasses were developed by micro-alloying, one with an additional content of 1 at.% Co and the other with 0.6 at.% Fe. The  $(\text{Pd}_{40}\text{Ni}_{40}\text{P}_{20})_{99}\text{Co}_1$  samples showed increased plasticity of about 50% compared to the ternary system in uniaxial compression experiments. On the other hand Fe addition immediately leads to an almost complete loss of ductility. The ultrasonic measurements did not show any significant change in the Poisson's ratios indicating that the ductility of BMGs is not adequately described by the Poisson's ratio alone. The impact of minor alloying on the fictive temperature, representing a measure of the amount of free volume, was analyzed. We found that the total amount of free volume frozen-in during vitrification is less important for the mechanical properties of bulk metallic glasses than the local distribution of free volume and thus the local atomic configurations. We have observed highly branched states with many secondary and tertiary shear bands involved for the ductile compounds. We suggest that the complex branching as a result of a modified local free volume distribution due to minor alloying prevents the primary shear bands from spreading further and thus the material from failure.

## Acknowledgment

We gratefully acknowledge financial support by the DFG via SPP 1594 (Topological engineering of ultra-strong glasses).

## Appendix A. Supplementary data

Supplementary data associated with this article can be found, in the online version, at <http://dx.doi.org/10.1016/j.scriptamat.2015.08.030>.

## References

- [1] M.F. Ashby, A.L. Greer, *Scr. Mater.* 54 (2006) 321–326.
- [2] C.C. Hays, C.P. Kim, W.L. Johnson, *Phys. Rev. Lett.* 84 (2000) 2901–2904.
- [3] F. Szeucs, C.P. Kim, W.L. Johnson, *Acta Mater.* 49 (2001) 1507–1513.
- [4] A. Donohue, F. Spaepen, R.G. Hoagland, A. Misra, *Appl. Phys. Lett.* 91 (2007) 241905.
- [5] J. Eckert, J. Das, S. Pauly, C. Duhamel, *J. Mater. Res.* 22 (2007) 285–301.
- [6] D.C. Hofmann, J.-Y. Suh, A. Wiest, G. Duan, M.-L. Lind, M.D. Demetriou, W.L. Johnson, *Nature* 451 (2008) 1085–1089.
- [7] R.L. Narayan, P.S. Singh, D.C. Hofmann, N. Hutchinson, K.M. Flores, U. Ramamurty, *Acta Mater.* 60 (2012) 5089–5100.
- [8] J. Schroers, W.L. Johnson, *Phys. Rev. Lett.* 93 (2004) 255506.
- [9] J.J. Lewandowski, W.H. Wang, A.L. Greer, *Philos. Mag. Lett.* 85 (2005) 77–87.
- [10] M.D. Demetriou, M.E. Launey, G. Garrett, J.P. Schramm, D.C. Hofmann, W.L. Johnson, R.O. Ritchie, *Nat. Mater.* 10 (2011) 123–128.
- [11] M.D. Demetriou, M. Floyd, C. Crewdson, J.P. Schramm, G. Garrett, W.L. Johnson, *Scr. Mater.* 65 (2011) 799–802.
- [12] X. Wang, Q.P. Cao, Y.M. Chen, K. Hono, C. Zhong, Q.K. Jiang, X.P. Nie, L.Y. Chen, X.D. Wang, J.Z. Jiang, *Acta Mater.* 59 (2011) 1037–1047.
- [13] Z.P. Lu, C.T. Liu, *J. Mater. Sci.* 39 (2004) 3965–3974.
- [14] W. Wang, *Prog. Mater. Sci.* 52 (2007) 540–596.
- [15] G. Kumar, D. Rector, R.D. Conner, J. Schroers, *Acta Mater.* 57 (2009) 3572–3583.
- [16] G. Kumar, S. Prades-Rodel, A. Blatter, J. Schroers, *Scr. Mater.* 65 (2011) 585–587.
- [17] G. Kumar, P. Neibecker, Y.H. Liu, J. Schroers, *Nat. Commun.* 4 (2013) 1536.
- [18] A.Q. Tool, C.G. Eichlin, *J. Am. Ceram. Soc.* 14 (1931) 276–308.
- [19] G. Wilde, G.P. Görlner, R. Willnecker, G. Dietz, *Appl. Phys. Lett.* 65 (1994) 397–399.
- [20] G. Wilde, G.P. Görlner, R. Willnecker, H.J. Fecht, *J. Appl. Phys.* 87 (2000) 1141–1152.
- [21] H. Blumenauer, *Werkstoffprüfung*, Deutscher Verlag für Grundstoffindustrie, 1989.
- [22] C. Gammer, C. Mangler, C. Rentenberger, H.P. Karnthaler, *Scr. Mater.* 63 (2010) 312–315.
- [23] B.J. Kestel, *Ultramicroscopy* 19 (1986) 205–211.
- [24] Y.P. Mitrofanov, M. Peterlechner, I. Binkowski, M.Y. Zadorozhnyy, I.S. Golovin, S.V. Divinski, G. Wilde, *Acta Mater.* 90 (2015) 318–329.
- [25] W.J. Wright, R.B. Schwarz, W.D. Nix, *Mater. Sci. Eng., A* 319–321 (2001) 229–232.
- [26] R. Maaß, D. Klaumünzer, J.F. Löffler, *Acta Mater.* 59 (2011) 3205–3213.
- [27] W.F. Wu, Y. Li, C.A. Schuh, *Philos. Mag.* 88 (2008) 71–89.
- [28] R.D. Conner, W.L. Johnson, N.E. Paton, W.D. Nix, *J. Appl. Phys.* 94 (2003) 904–911.
- [29] E. Ma, *Nat. Mater.* 14 (2015) 547–552.
- [30] E. Lambson, W. Lambson, J. Macdonald, M. Gibbs, G. Saunders, D. Turnbull, *Phys. Rev. B* 33 (1986) 2380–2385.
- [31] Y. He, T. Shen, R.B. Schwarz, *Metall. Mater. Trans. A* 29 (1998) 1795–1804.